ELSEVIER

Ultramicroscopy 78 (1999) 141–151

ultramicroscopy

Towards atomic column-by-column spectroscopy

B. Rafferty*, S.J. Pennycook

Solid State Division, Oak Ridge National Laboratory, P.O. Box 2008, Oak Ridge, TN 37831-6030, USA

Received 9 November 1998; received in revised from 9 February 1999

Abstract

The optical arrangement of the scanning transmission electron microscope (STEM) is ideally suited for performing analysis of individual atomic columns in materials. Using the incoherent *Z*-contrast image as a reference, and arranging incoherent conditions also for the spectroscopy, a precise correspondence is ensured between features in the inelastic image and elastic signals. In this way the exact probe position needed to maximise the inelastic signal from a selected column can be located and monitored during the analysis using the much higher intensity elastic signal. Although object functions for EELS are typically less than 1 Å full-width at half-maximum, this is still an order of magnitude larger than the corresponding object functions for elastic (or diffuse) scattering used to form the *Z*-contrast image. Therefore, the analysis is performed with an effective probe that is significantly broader than that used for the reference *Z*-contrast image. For a 2.2 Å probe the effective probe is of the order of 2.5 Å, while for a 1.3 Å probe the effective probe is 1.6 Å. Such increases in effective probe size can significantly reduce or even eliminate contrast between atomic columns that are visible in the image. However, this is only true if we consider circular collector apertures. Calculations based upon the theory of Maslen and Rossouw [Maslen and Rossouw, Philos. Mag. 49 (6) (1984) 735–742; Rossouw and Maslen, Philos. Mag. 49 (6) (1984) 743–757] show that employing an annular collector aperture can reduce the FWHM of the inelastic object function down to values close 0.1 Å. With practical collector aperture sizes it should be possible to achieve this increased spatial resolution without losing too much signal.

1. Introduction

Internal interfaces are known to dominate the structure–property relationships of many materials and devices. Thus, the ultimate goal of all atomic or near atomic resolution analysis techniques is to determine both the physical and electronic structure of defects, such as a dislocation core or an interface, within a crystalline matrix with atomic column sensitivity. The optical arrangement in the HB603U STEM is ideally suited for performing analysis of individual atomic columns in materials. The major strength of this instrument is that with incoherent *Z*-contrast imaging it is possible to obtain direct structure images of the atomic configuration of the specimen. One can directly image defects within a sample and determine the physical structure of the sample on-line without having to rely on any post acquisition image processing techniques. Using the incoherent *Z*-contrast image as a reference, and arranging incoherent conditions for the spectroscopy, a precise correspondence is ensured between features in the inelastic and elastic

*Corresponding author. Cavendish Laboratory, Madingley Road, Cambridge CB3 0HE, UK. Fax: +44-1223-337333.

E-mail address: berll@cus.cam.ac.uk (B. Rafferty)

0304-3991/99/$ - see front matter
PII: S0304-3991(99)00033-9

signals. In this way the exact probe position needed to maximise the inelastic signal from a selected column can be located and monitored during the analysis using the much higher intensity elastic scattering. Electron energy loss spectroscopy (EELS) analysis offers many advantages over X-ray spectroscopy, such as high collection efficiency and the ability to analyse near edge fine structure. Thus, integrating the HB603U with a dedicated McMullan-type PEELS system will spawn an instrument with unique performance [1].

Defining incoherent imaging conditions for the EELS means that the probe can be separated out of the expression for the inelastic intensity, and the real space distribution of scattering power is then referred to as the object function. The inelastic image is then given by the convolution of the probe intensity profile with the object function. As these functions are similar to Gaussians in many cases, the best single measure of resolution is the FWHM, as convoluting two Gaussians leads to a Gaussian with FWHM equal to the individual two summed in quadrature. However, although object functions for EELS are typically less than 1 Å FWHM, this is still an order of magnitude larger than the corresponding object functions for elastic (diffuse) scattering used to form the *Z*-contrast image. Therefore, the analysis is performed with an effective probe that is significantly broader than that used for the reference *Z*-contrast image. For a 2.2 Å probe the effective probe is of the order 2.5 Å, while for a 1.3 Å probe the effective probe is 1.6 Å. Such increases in the effective probe size can significantly reduce or even eliminate the contrast between atomic columns that are visible in the image. A sub-angstrom probe is thus more essential for atomic resolution analysis than it is for imaging. It may be possible to avoid this larger effective probe size if we could set up the experimental conditions to produce an object function with a smaller FWHM. A possible method to achieve this was indicated by Kohl and Rose [2] and explicitly outlined by Ritchie and Howie [3].

The calculations presented by Kohl and Rose illustrated an increase in the localisation of the inelastic signal with the use of a larger collection aperture, while Ritchie and Howie suggested that the use of an off-axis collector aperture would increase the spatial resolution of the inelastic signal. By removing the low angle inelastic scattering events from the electrons forming the spectrum or inelastic image it should be possible to reduce the size of the effective probe used for the analysis. This can be achieved experimentally by using an annular collector aperture. Here we present calculations of the inelastic object function for K-shell ionisation based upon the non-relativistic theory of Maslen and Rossouw [4–6] for both circular and annular collector apertures. Although we have a 300 kV beam and are using a non-relativistic theory we feel that the results will provide a qualitative idea of the various effects discussed. One of the main differences between this approach and previous object function (actually response function) calculations is that we include the full quantum mechanical nature of the matrix elements describing the transitions. In other calculations [2,7] these matrix elements have been replaced by some approximation that removes their structure at higher scattering angles; in reality, the matrix elements are not constant over all scattering angles. We briefly discuss the methodology of this theory, point out some of its limitations and how it could be extended to include effects such as multiple scattering. The *Z*-dependence of the FWHM of the object functions and how this relationship changes with collector aperture geometry will be presented as will the beam energy dependence of the object functions. The practical limitations to the use of annular collector apertures such as the physical limitations to the aperture sizes within the HB603U and the potential loss of signal will also be outlined. This last point will also be discussed in the context of high angle plasmon imaging. Firstly, we shall outline the ideas of incoherent *Z*-contrast imaging to show how we can relate the elastic signal to the inelastic signal by the use of an effective probe.

2. Incoherent *Z*-contrast imaging

It has been shown [8] that by using a large high angle annular detector to collect the elastically scattered electrons a *Z*-contrast image can be produced which has an implicitly higher spatial resolution than that of a conventional high-resolution

bright field image. This difference comes from the fact that with the large annular detector in reciprocal space we are summing incoherently over many pairs of overlapping Bragg diffracted discs. Thus, we can separate the integration's over the partial plane-waves forming the probe and that of the wavevector defining the direction of the scattered electron. Fourier transforming back to real space now leaves us with an image which can be written as a convolution

$$I_{\mathrm{ADF}}(\boldsymbol{R}_0) = |P(-\boldsymbol{R}_0)|^2 \otimes |o(\boldsymbol{R}_0)|^2, \quad (1)$$

where $P(\boldsymbol{R}_0)$ is the complex amplitude of the probe and $|o(\boldsymbol{R}_0)|^2$ is the object function of the scattering centre. In contrast to this the intensity in a conventional high-resolution image may be written as

$$I_{\mathrm{BF}}(\boldsymbol{R}_0) = |P(-\boldsymbol{R}_0) \otimes o(\boldsymbol{R}_0)|^2, \quad (2)$$

where $o(\boldsymbol{R}_0)$ is the inverse Fourier transform of the matrix element describing the scattering event. It can be clearly seen that with incoherent Z-contrast imaging the image interpretation is much more straightforward and the atomic configuration of the sample can be directly imaged. Since the object functions are so narrow ($\leqslant 0.1$ Å) we can approximate them as being delta functions. Thus, the contrast and resolution in the image is dictated by the probe profile. The optical arrangement of the high-resolution STEM allows these incoherent conditions to be established simultaneously for the collection of elastically and inelastically scattered electrons. Consequently, the same theory for the incoherent Z-contrast imaging will hold true for that of inelastic imaging. For the inelastic case we have object functions that cannot be approximated as delta functions. The additional width of the object function is now going to smear out the probe profile. We can, however, interpret this image in a similar fashion to the elastic case as follows. Since the image is given by a convolution, we may replace the object functions by delta functions if we replace the probe profile by an effective probe whose width is larger than the original probe. The effective probe is simply the original probe convoluted with the real space object function. Although this effective probe may not be much broader than that for the elastic image the slightest increase in width can significantly reduce or even eliminate contrast between the atomic columns that we intend to analyse. We need to reduce the size of the effective probe in order to perform both image and EELS analysis on the 1 Å scale.

The question of what detector angle is sufficiently high for incoherent imaging to be a good assumption was discussed for the elastic case by Jesson and Pennycook [9]. They proposed a minimum detector aperture θ_{i} to achieve incoherent imaging of two objects separated by ΔR of $\theta_{\mathrm{i}} = 1.22\ \lambda/\Delta R$, where the detected intensity varies by less than 5% from that calculated assuming incoherent imaging. In the inelastic case we also have the energy loss process itself to localise the scattering and break coherence, so this criterion may be too severe. In this paper we assume that incoherent imaging applies and that the probe and object function can therefore be separated. For the smallest detector angles we consider, we expect the error in the inelastic image resolution to be well below 5%.

3. Calculating the inelastic object functions

Much work has been carried out developing theories to model and calculate the inelastic object function and use them to investigate the inelastic imaging process [4–6,10–12]. Here we use the theory of Maslen and Rossouw [4,5] as this model provides analytical solutions that are simply evaluated and will be summarised here. As is usual we describe the incident and scattered fast electron as plane waves with wavevectors $\boldsymbol{k}$ and $\boldsymbol{k}'$, respectively. The incident fast electron is scattered from an isolated atom in which the atomic 1s electron is ejected from the atom. The momentum of this ejected electron is not fixed by the momentum transferred from the fast electron to the atom, $\hbar(\boldsymbol{k} - \boldsymbol{k}')$, but is distributed over a range of directions that reflect the momentum distribution of the 1s state. A hydrogenic model of the atom is used to provide analytical formulae for the matrix elements. Implicit within the expression for the matrix elements is an integration over all possible directions, κ, of the ejected atomic electron since this is not detected and we have no knowledge of its momentum. The

dipole approximation is not used within this model and so it is valid for all scattering angles of the incident fast electron. Fig. 1 shows a schematic of the scattering process including all relevant vectors. In this framework the object function in reciprocal space is (using notation from the Maslen and Rossouw papers) defined as

$$\tilde{O}(\boldsymbol{Q}) = \int \frac{2|F(1s,1s)|q_{\perp}}{Q_1^2 Q_2^2}\,\mathrm{d}\theta\,\mathrm{d}\phi, \tag{3}$$

where θ and ϕ define the collector aperture. $F(1s,1s)$ is given by

$$F(1s,1s) = 512\,\pi^3 Z^5 \left(\frac{(Q_1^2+(Z-\chi)^2)(Q_2^2+(Z-\chi)^2)}{(Q_1^2+(Z+\chi)^2)(Q_2^2+(Z+\chi)^2)}\right)^{Z/2\chi} \frac{H}{PR}, \tag{4}$$

where

$$H = \left\{ \begin{array}{l} \left[\dfrac{-1}{W^3}\left(\dfrac{WZ\cos(\psi)}{\chi} + T\sin(\psi)\right)\right] \times \left(\begin{array}{l} PR - \alpha_1^2 R - \alpha_2^2 P + \alpha_1\alpha_2 T \\ + 2Q_2^2(\alpha_1 T - \alpha_2 P) + 2Q_1^2(\alpha_2 T - \alpha_1 R) \\ + 3T\dfrac{(\alpha_1 T - \alpha_2 P)(\alpha_2 T - \alpha_1 R)}{W^2} \end{array} \right) \\ \\ + \dfrac{\sin(\psi)}{W}\left(4Q_1^2Q_2^2 - (\alpha_1 T - \alpha_2 P)(\alpha_2 T - \alpha_1 R)\dfrac{(Z^2-\chi^2)}{\chi^2 W^2}\right) \end{array} \right\} \tag{5}$$

and

$$\alpha_m = Q_m^2 - \chi^2 + Z^2, \qquad P = \alpha_1^2 + 4\chi^2 Q_1^2,$$

$$R = \alpha_2^2 + 4\chi^2 Q_2^2, \qquad T = \alpha_1\alpha_2 + 4\chi^2 \boldsymbol{Q}_1.\boldsymbol{Q}_2,$$

$$W^2 = PR - T^2, \qquad \psi = \frac{Z}{\chi}\tan^{-1}\left(\frac{W}{T}\right),$$

$$\boldsymbol{Q}_1 = -\tfrac{1}{2}\boldsymbol{Q} + \boldsymbol{q}, \quad \boldsymbol{Q}_2 = \tfrac{1}{2}\boldsymbol{Q} + \boldsymbol{q}. \tag{6}$$

$\boldsymbol{Q}$ is a vector lying in the plane of the aperture and $\boldsymbol{q} = \boldsymbol{k}' - \boldsymbol{k}$. Z is a measure of the screened atomic charge and $\chi = \mathrm{i}\kappa$ and an energy of 50 eV has been assigned to the ejected electron above the ionisation threshold. The real space object function $|o(\boldsymbol{R}_0)|^2$ is the Fourier transform of $\tilde{O}(\boldsymbol{Q})$.

There are some obvious limitations to this model such as using hydrogenic wavefunctions. The use of Hartree–Fock wavefunctions would provide a better description of the atomic system which Oxley and Allen are continuing with at present [13]. It is not yet clear from this work, however, how the object functions are modified by the use of the Hartree–Fock wavefunctions. Since we are integrating over all directions of the ejected electron we have assumed a free electron density of states for this electron which, as pointed out by Saldin and Rez [14], omits any modelling of fine structure effects. Despite these limitations we feel that this model should still provide much insight into the effect of collector aperture geometry on the structure of the inelastic object functions.

Another important point is that we do not use any approximations for the matrix elements. It is usually assumed [2,7] that the matrix elements do not vary much with scattering angle and so can often be ignored to a first approximation. However, Fig. 2 shows plots for the term $F(1s,1s)$ $[=\langle \mathrm{i}|\exp(\mathrm{i}\boldsymbol{q}.\boldsymbol{r})|f\rangle\langle f|\exp(\mathrm{i}\boldsymbol{q}.\boldsymbol{r})|i\rangle]$ in reciprocal space for different scattering angles. It can be clearly seen that for all values of Q and scattering angle θ the matrix elements are not constant. Only for small scattering angles (<5 mrad) could this approximation be used; it is clearly invalid for the larger angles that are necessary for incoherent conditions. We

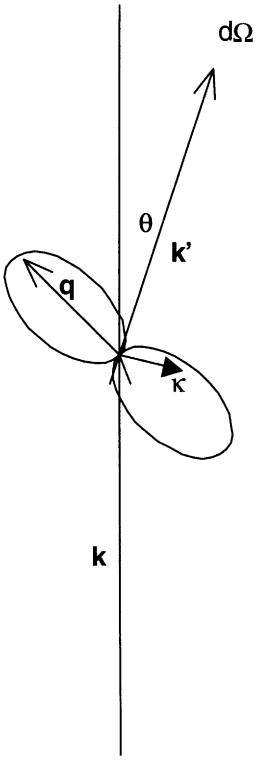

Fig. 1. Schematic diagram showing the inelastic scattering process.

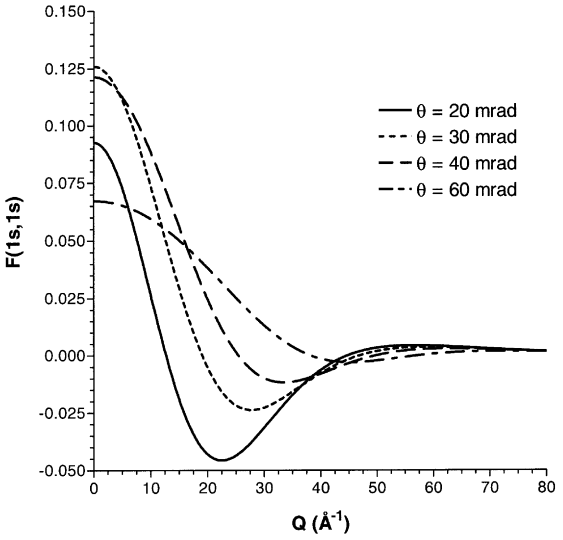

Fig. 2. Plot in reciprocal space of how the matrix elements for the inelastic scattering of a fast electron from an oxygen atom vary for different collection angles θ.

will find that this will make a significant difference to the widths of the object functions.

4. Results of simulations

4.1. Circular collector apertures

Fig. 3 shows a plot of the variation of the FWHM of the inelastic object function for different collector aperture sizes and atomic number. It can be seen that the width of the object function is decreased as the ionisation energy is increased. This is in agreement with the results of Kohl and Rose [2] although they plot a response function that includes a probe profile as well as the object function. It can also be seen that increasing the size of the collector aperture for fixed ionisation energy will also reduce the width of the object functions. Fig. 4 shows that as the collector aperture size is increased the large angle scattering contributes more to the high Q regions of the object functions in reciprocal space. As was pointed out by Kohl and Rose [2] this is because we are collecting the electrons that have passed closer to the nucleus and so are contributing the high spatial resolution information to the object function. It is the exploitation of this property that leads to the use of the annular collector apertures to further reduce

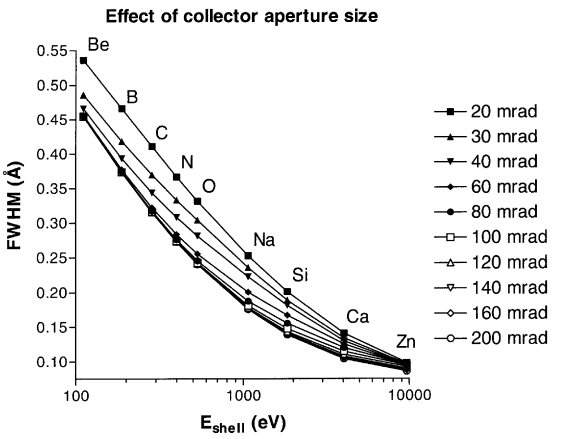

Fig. 3. Plot to show the variation of the FWHM of the inelastic object functions for different collector aperture sizes and atomic number.

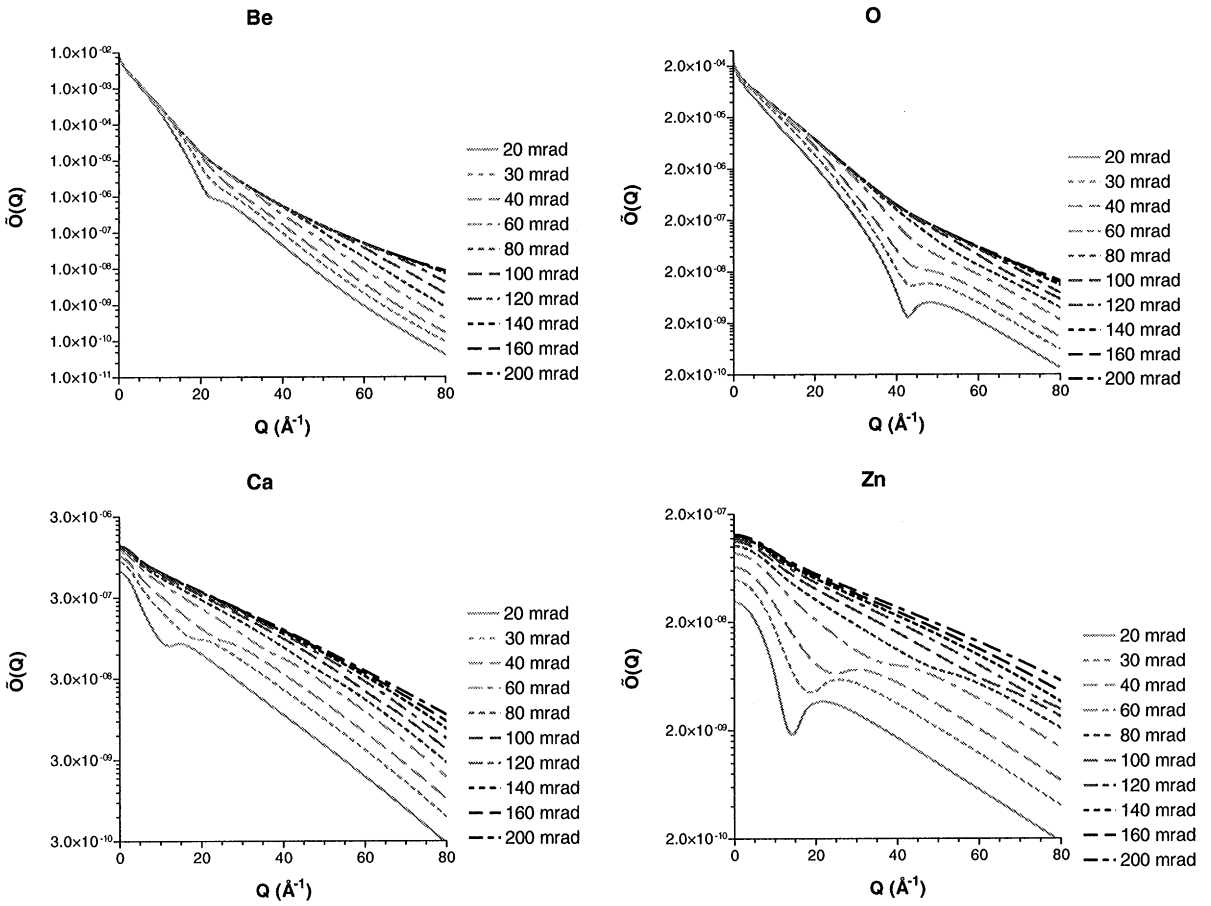

Fig. 4. Plots of the object functions in reciprocal space showing how the increased collector aperture sizes increases the contributions to the larger Q regions. This additional contribution is proportionally larger for the lighter atoms.

the widths of the inelastic object functions. It can also be seen that this contribution is proportionally larger for lighter atoms. The $\tilde{O}(\boldsymbol{Q})$ falls by 2 and 8 orders of magnitude with a 20 mrad collector aperture for Zn and Be, respectively, while for a 200 mrad collector aperture the corresponding figures are 1 and 5 orders of magnitude. It is the exploitation of this property that leads to the use of the annular collector apertures to further reduce the widths of the inelastic object functions.

4.2. Annular collector apertures

In Fig. 5 we show the oxygen object function in reciprocal space for the individual annuli building up from a 20 to 200 mrad collector aperture. The contributions from an annular section changes quite drastically as the inner and outer radii are increased by the same amount. The small angle annular sections contribute quite strongly at $Q = 0\ \text{Å}^{-1}$. As the inner angle is increased the low Q contributions become diminished while the large Q contributions are strengthened. Consequently, the FWHM of the oxygen real space object functions for annuli of 20–40 and 80–100 mrad are 0.231 and 0.091 Å, respectively. The larger annular sections contain more high-resolution information.

A striking result that comes from the use of annular collector apertures is the change in the

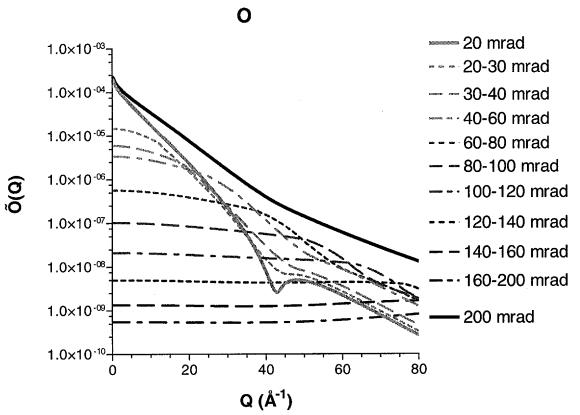

Fig. 5. The oxygen object function in reciprocal space showing the contributions from the different annuli as we increase from 20 to 200 mrad.

Z-dependence of the FWHM of the object functions. It is possible using a sufficiently large inner radii annular collector aperture to produce an object function for a low Z atom that has a smaller FWHM than that of a larger Z atom see Fig. 6. The reciprocal space object functions for low Z atoms have a very narrow distribution and fall off much more quickly than the corresponding high Z atoms for circular collector apertures. When the inner angle (θ_{inner}) is increased all contributions with $Q \leqslant 2q\cos(\theta_{\text{inner}})$ are suppressed. The low Z atoms are affected the most since their $\tilde{O}(Q)$ fall off so strongly with Q. Further increasing the inner angle can push the contribution of the low Q regions of the light atoms below that of heavier atoms (Fig. 7) while their high Q contributions are comparable in value. This reduction of the low Q parts removes the large tails present in the real space object functions of the light atoms. Thus, the lighter atoms can have a FWHM that is smaller than heavier atoms.

4.3. Beam energy dependence of the object functions

Changing the energy of the fast incident electron alters the sizes of the object functions. We see in Fig. 8 that, for oxygen K-shell ionisation, increasing the beam energy will decrease the size of the object functions for both circular and annular collector apertures. According to classical mechanics using a higher energy incident electron should allow the 1s atomic electron to be excited from further away [15]. The maximum distance from which the electron can excite an electron is proportional to the velocity of the incident electron. Thus, increasing the beam energy by a factor of 3 should surely increase the widths of the object functions. However, increasing the beam energy also means that the incident electron is able to pass much closer to the nucleus of the atom and so this should reduce the widths of the object functions. If these variations in the range of possible impact parameters are weighted with the corresponding probability of producing the required excitation then we find that the overall effect is to reduce the size of the average impact parameter with increased beam energy.

4.4. Possible limitations to the use of annular collector apertures

We have seen in these calculations that it is possible in principle to reduce the FWHM of the object functions down to values close to 0.1 Å. However, this was only possible by using annular collector apertures with outer radii approaching 200 mrad! If we are to use the incoherent Z-contrast image as a reference during the acquisition of these spectra the choice of collector aperture size will be dictated by the inner angle of the annular dark field detector (approx. 30–40 mrad). This means that for say oxygen we can reduce the width of the object function from 0.33 to 0.23 Å. Although this is not as striking as that which could be achieved with larger annular collector apertures this may be enough to allow one to distinguish between two columns of oxygen that are separated by only 1.5 Å. This would still be quite an achievement!

The use of an annular collector aperture means that we cut out the low angle scattering from the spectrum. This may mean that we do not have enough signal to collect to fully exploit the advantage of the annular collector apertures. However, Fig. 9 shows oxygen object functions for a circular collector aperture and the proposed annular collector apertures. The peak intensity for the annular collector apertures is only reduced slightly from

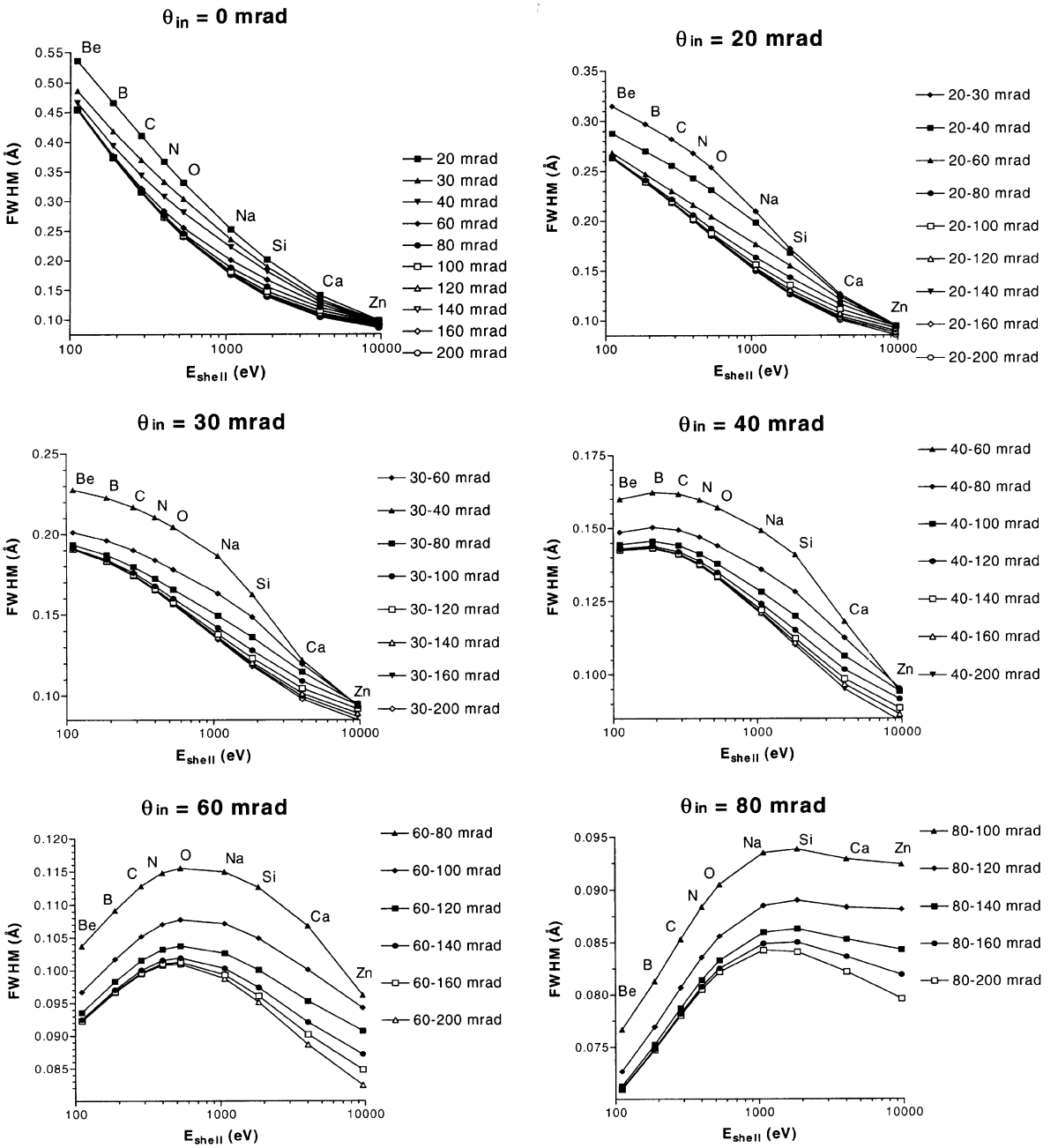

Fig. 6. Plots to show the variation in the Z-dependence of the FWHM with the use of different sized annular collector apertures.

that of the circular collector aperture, because we are losing primarily the undesirable tails of the object function. Such tails contribute to the total detected signal, but being delocalised are not useful for atomic resolution studies. The decrease in total collected signal will be compensated by the increased contrast that comes from removing the delocalised background.

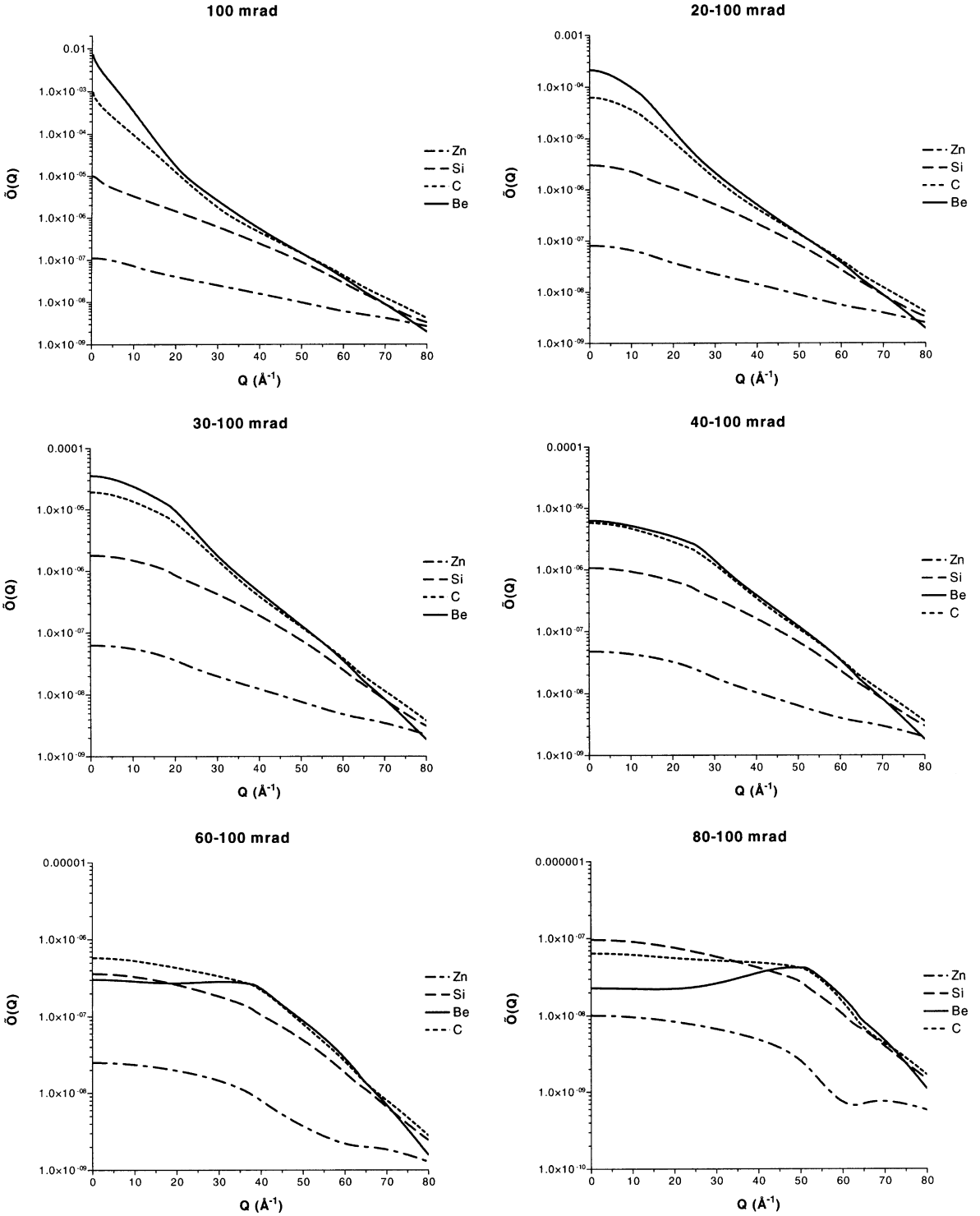

Fig. 7. Reciprocal space object functions. Increasing the inner angle suppresses the low Q regions for light atoms more so than for heavier atoms.

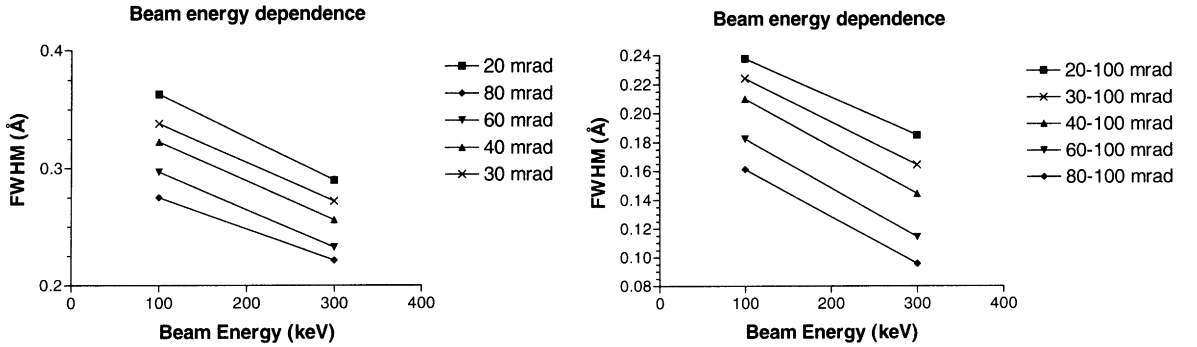

Fig. 8. Beam energy dependence on the object functions of oxygen.

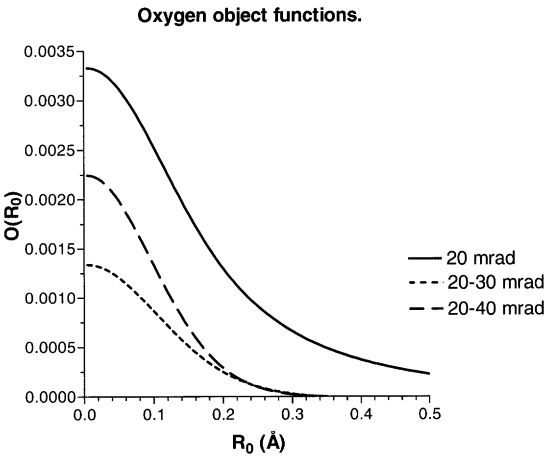

Fig. 9. Object functions for oxygen K-shell. The use of the annular collector aperture does not reduce the peak intensity too drastically from that for the circular collector aperture.

If it were possible to use the much larger annular collector apertures and the low signal was not a limiting factor we would be able to get the spatial resolution that the calculations would imply. The problem that we would encounter would be that of multiple scattering effects. This is not included within these calculations. If we compare the probability of a single inelastic scattering event to a large angle ($>$ 40 mrad) and that of a single low angle inelastic event followed by a high angle elastic event, or vice versa, we would find that the second scenario is more probable. We would still obtain a high spatial resolution but this would be because of the *elastic* scattering contribution. This will probably have some significant implications on the interpretation of atomic resolution plasmon imaging at surfaces [7]. In our case we can simply place the probe in specific locations within the unit cell to measure the inelastic image contrast. Comparing this with the elastic image contrast we will be able to accurately quantify the loss of contrast due to delocalisation (i.e. the effective probe broadening).

5. Conclusions

We have briefly outlined the theory of Maslen and Rossouw and mentioned some of its limitations. Using their approach, we have calculated the inelastic object functions for both circular and annular collector apertures, specifically including the variation of the matrix elements with scattering angle. The effects of the size of the inner angle of the annular collector apertures, the Z-dependence and the beam energy dependence on the FWHM of the object functions have been discussed. It was shown that it is possible that with annular collector apertures it is possible for the lighter Z atoms to have a real space object with a smaller spatial extent than a larger Z atom. This result was explained by the greater proportional suppression of the low Q regions of the reciprocal space object functions. Contrary to classical impact parameters, increasing the beam energy actually reduces the widths of the real space object functions due to the incident electron being able to approach the nucleus much more

closely. The limitations and practicalities of the use of annular collector apertures have been pointed out and the possible effects of multiple scattering were discussed. Experiments are necessary to see if annular collector apertures are useful in practice for improving spatial resolution in EELS.

Acknowledgements

The authors would like to thank P.D. Nellist for fruitful discussions related to this work. This research was supported by Lockheed Martin Energy Research Corp. under DOE Contract No. DE-AC05-96OR22464, and by appointments to the ORNL Postdoctoral Research Associates Program administered jointly by ORNL and ORISE.

References

[1] B. Rafferty, Probing electronic structure in the region of the bandgap using electron energy loss spectroscopy, Ph.D. Thesis, Cambridge University, 1997.
[2] H. Kohl, H. Rose, Theory of image formation by inelastically scattered electrons in the electron microscope, 1985.
[3] R.H. Ritchie, A. Howie, Inelastic-scattering probabilities in scanning-transmission electron microscopy, Philos. Mag. 58 (5) (1988) 753.
[4] V.W. Maslen, C.J. Rossouw, The inelastic-scattering matrix element and its application to electron-energy loss spectroscopy, Philos. Mag. 47 (1) (1983) 119.
[5] V.W. Maslen, C.J. Rossouw, Implications of (e,2e) scattering for inelastic electron-diffraction in crystals 1. Theoretical, Philos. Mag. 49 (6) (1984) 735.
[6] C.J. Rossouw, V.M. Maslen, Implications of (e, 2e) scattering for inelastic electron-diffraction in crystals 2. Application of the theory, Philos. Mag. 49 (6) (1984) 743.
[7] D. Muller, J. Silcox, Delocalisation in inelastic scattering, Ultramicroscopy 59 (1995) 195.
[8] P.D. Nellist, S.J. Pennycook, Accurate structure determination from image reconstruction in ADF STEM, J. Microsc. Oxford 190 (Part 1/2) (1998) 159.
[9] D.E. Jesson, S.J. Pennycook, Incoherent imaging of thin specimens using coherently scattered electrons, Proc. Roy. Soc. London A 441 (1993) 261.
[10] L.J. Allen, I.E. McCarthy et al., Effects of diffraction on the (E, 2e) reaction in crystals, Aust. J. of Phys. 43 (4–5) (1990) 453.
[11] O.F. Holbrook, D.M. Bird, Theoretical modelling of atomic images formed with inelastically scattered electrons, Inst. Phys. Conf. Ser. 147 (1995) 175.
[12] O. Holbrook, Diffraction effects in inelastic imaging, Phys. Ph.D., University of Bath, 1997.
[13] Oxley L. Allen, Private communication 1998.
[14] D.K. Saldin, P. Rez, The theory of the excitation of atomic inner-shells in crystals by fast electrons, Philos. Mag. B 55 (1987) 481.
[15] J.D. Jackson, Classical Electrodynamics, Wiley, New York, 1975.